Volume 61
Number 11
7 February 2025
Pages 2145–2362

ChemComm

Chemical Communications

rsc.li/chemcomm

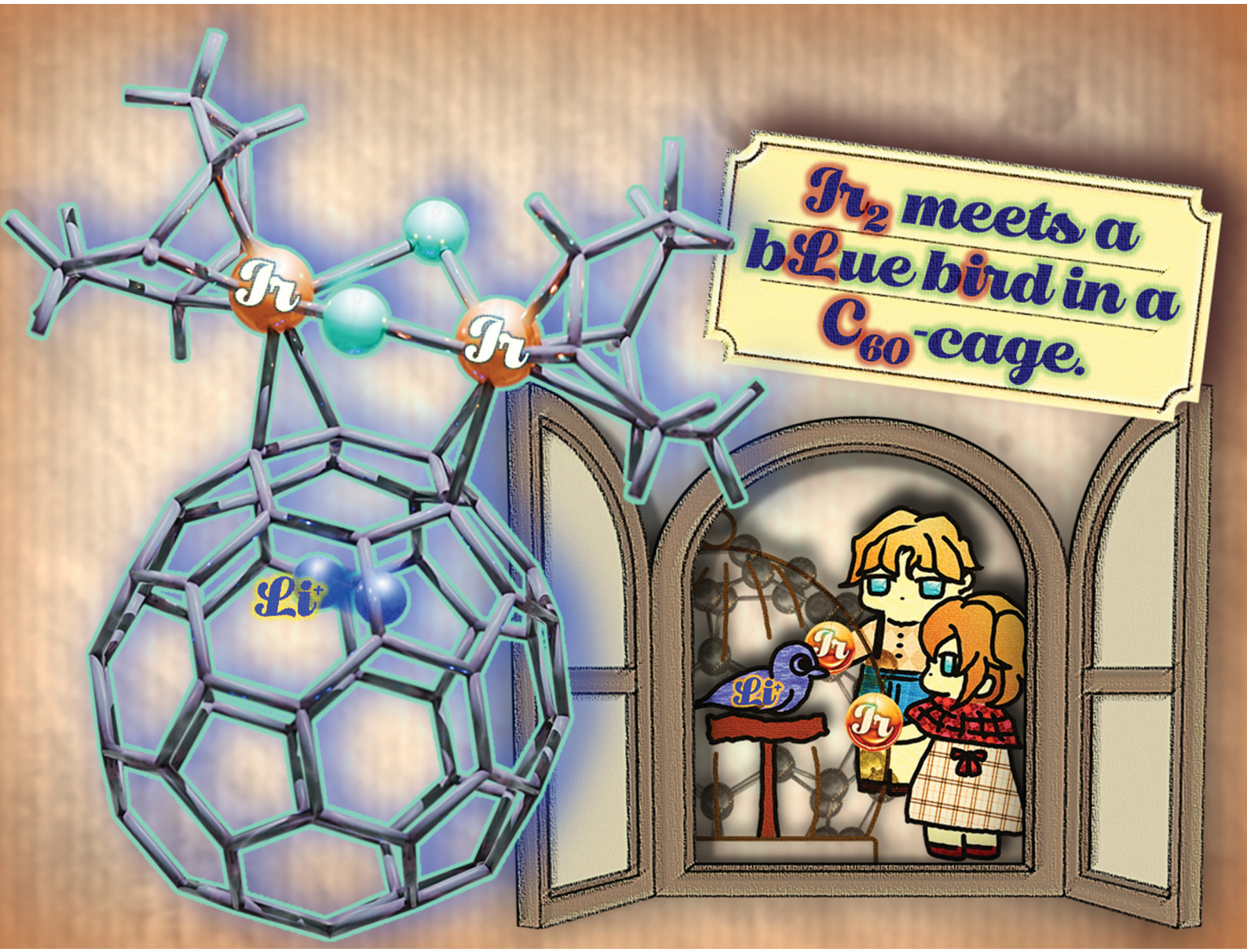

ISSN 1359-7345

ROYAL SOCIETY OF CHEMISTRY

COMMUNICATION

Takashi Komuro, Hisako Hashimoto *et al.*

Dinuclear iridium complexes ligated by lithium-ion endohedral fullerene $Li^+@C_{60}$

ChemComm

COMMUNICATION

View Article Online
View Journal | View Issue

Cite this: *Chem. Commun.*, 2025, **61**, 2273

Received 15th October 2024,
Accepted 29th November 2024

DOI: 10.1039/d4cc05485g

rsc.li/chemcomm

Dinuclear iridium complexes ligated by lithium-ion endohedral fullerene $Li^+@C_{60}$†

Chinari Fukushi, Takashi Komuro * and Hisako Hashimoto *

The diiridium complexes of lithium-ion endohedral fullerene $Li^+@C_{60}$ were synthesised in high yields. X-ray crystallography revealed the η^2:η^2-coordination of $Li^+@C_{60}$ and the disorder of the Li^+ ion over two sites close to the coordinated carbons. ^{13}C NMR study suggested the presence of dynamic behaviour *via* haptotropic rearrangements. UV/Vis and CV characteristics were also investigated experimentally and theoretically.

Donor–acceptor complexes consisting of a transition metal (TM) donor and an organic acceptor have gained significant attention owing to their wide range of applications in materials engineering,[1] molecular electronics,[2] catalytic chemistry, *etc.*[3] Adducts of electron-rich TM units with fullerene C_{60} can be viewed as donor–acceptor molecules and are potential candidates for excellent building blocks of such materials.[4] However, developing highly functional materials based on C_{60}–TM complexes faces several challenges. For instance, the addition of multi-metal centres to the C_{60} shell is likely to result in the formation of multiple regioisomers because the entire surface of C_{60} can act as a reaction site.[5] Moreover, electrically neutral C_{60} tends to easily aggregate because of its low solubility in various organic solvents,[6] leading to low yields of C_{60}–TM complexes and difficulties in isolation/characterisation. Therefore, it is necessary to develop a method for the selective synthesis of highly soluble single complexes.

From this perspective, lithium-ion endohedral fullerene $Li^+@C_{60}$[7] is a promising molecule for selective synthesis because $Li^+@C_{60}$ has higher electron acceptability relative to C_{60} due to the electrostatic interaction between the Li^+ ion and the C_{60} carbons.[8] Consequently, $Li^+@C_{60}$ readily reacts with electron-rich TM fragments to form $Li^+@C_{60}$–TM complexes as demonstrated using mononuclear metal fragments [Fig. 1(a), **A**–**C**].[9] These complexes exhibit greater stability compared with the corresponding C_{60} analogues due to the formation of strong C_{60}–TM bonds based on the stronger π-back-donation from TM (donor) to C_{60} (acceptor) [Fig. 1(b)].[10] Moreover, the ionic nature of $Li^+@C_{60}$ allows the improvement of its solubility, modifying counter anions with high affinity toward organic solvents.[11] Therefore, $Li^+@C_{60}$–TM complexes could offer access to unique molecular structures and properties that are inaccessible by use of C_{60} analogues. In this context, we recently became interested in $Li^+@C_{60}$–TM complexes with multi-metal units. In these complexes, the donor–acceptor interaction between the TM and fullerene units and the electrostatic interaction between the C_{60} cage and endohedral Li^+-ion should be further modulated by π-back-donation from the multi-metal centres.

As the first example of a multi-metallic C_{60}–TM complex, the tetrairidium complex $C_{60}\{Ir_2Cl_2(cod)_2\}_2$ (**D**) (cod = 1,5-cyclooctadiene) has been previously obtained as a low-solubility product.[12] However, no isolated yield or detailed properties, except the crystal structure, have been reported. Inspired by this example, we recently performed reactions of $Li^+@C_{60}$ with three halogen-bridged diiridium complexes, $Ir_2X_2(cod)_2$ (X = Cl, Br and I). Herein, we report the synthesis of dinuclear $Li^+@C_{60}$–

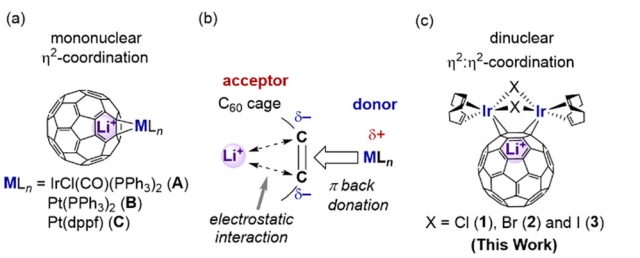

Fig. 1 (a) Previously-reported $Li^+@C_{60}$–TM complexes.[9] (b) Schematic diagram of the electrostatic interaction between the C_{60} cage and metal fragments ML_n. (c) Illustration of the $Li^+@C_{60}$–$[Ir_2]$ complexes in this work.

Department of Chemistry, Graduate School of Science, Tohoku University, Sendai 980-8578, Japan. E-mail: takashi.komuro.c5@tohoku.ac.jp, hisako.hashimoto.b7@tohoku.ac.jp

† Electronic supplementary information (ESI) available: Synthetic and experimental procedures, characterisation data, details of X-ray crystallographic analysis, NMR spectra and theoretical calculations. CCDC 2389980 (for **1**), 2389981 (for **2**) and 2389982 (for **3**). For ESI and crystallographic data in CIF or other electronic format see DOI: https://doi.org/10.1039/d4cc05485g

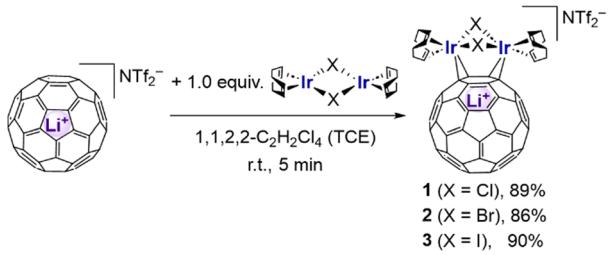

Scheme 1 Synthesis of $Li^+@C_{60}$-diiridium complexes **1–3**.

TM complexes, $[\{\mu\text{-}\eta^2{:}\eta^2\text{-}(Li^+@C_{60})\}\{Ir_2X_2(cod)_2\}](NTf_2^-)$ [X = Cl (**1**), Br (**2**) and I (**3**); Tf = CF_3SO_2], and their solid-state structures and spectroscopic properties in solution [Fig. 1(c)].

The reaction of $[Li^+@C_{60}](NTf_2^-)$ with 1 equiv of $Ir_2Cl_2(cod)_2$ in 1,1,2,2-tetrachloroethane (TCE) for 5 min at room temperature afforded almost quantitatively $[\{\mu\text{-}\eta^2{:}\eta^2\text{-}(Li^+@C_{60})\}\{Ir_2Cl_2(cod)_2\}](NTf_2^-)$ (**1**). Complex **1** was isolated as black crystals in 89% yield (Scheme 1). Using $Ir_2Br_2(cod)_2$ and $Ir_2I_2(cod)_2$ instead of $Ir_2Cl_2(cod)_2$, the corresponding complexes **2** and **3** were isolated in 86% and 90% yields, respectively. Complexes **1–3** showed good solubility in various organic solvents [CH_2Cl_2, THF, 1,2-dichlorobenzene (*o*-DCB), *etc.*], which enabled us to collect multiple spectroscopic data in solution, including ^1H, ^7Li and ^{13}C NMR, as well as UV/Vis and cyclic voltammetry (CV), in addition to their solid-state structures.

The crystal structures of complexes **1–3** were determined using single-crystal X-ray diffraction (SC-XRD). As shown in Fig. 2(a) for **1**, and Fig. S2 and S3 (ESI†) for **2** and **3**, respectively, it was unambiguously revealed that each complex had an $[Ir_2]$ unit coordinated by the $Li^+@C_{60}$ shell in an $\eta^2{:}\eta^2$-fashion. For example, the four Ir–C(C_{60}) distances of **1** are 2.170(4), 2.162(4), 2.169(4) and 2.170(4) Å [Fig. 2(b)], which indicate the $\eta^2{:}\eta^2$-coordination to the two iridium atoms at the [6 : 6] positions of the C_{60} shell. The average values of the four bond distances, **1** [av. 2.168(2) Å] is comparable with those of **2** [av. 2.169(2) Å] and **3** [av. 2.183(4) Å] (Table S2, ESI†), which are significantly shorter than that of non-Li^+ encapsulated C_{60}-iridium complex **D** [av. 2.218(3) Å].[12] Moreover, the three C–C bond distances at the C1–C2–C3–C4 moiety of **1** are lengthened by 6–8% upon coordination, relevant to the corresponding values of $Li^+@C_{60}$ (1.39 and 1.45 Å at the [6 : 6] and [6 : 5] positions, respectively) [Fig. 2(b)]. These C–C distances at the C1–C2–C3–C4 moiety were almost the same on average among the three complexes [av. 1.506(3) (**1**), av. 1.508(3) (**2**) and av. 1.511(6) (**3**) Å], and are significantly longer than that of **D** [av. 1.487(6) Å].[12] Thus, the π-back-donation from the two Ir centres to the C_{60} shell in **1–3** is estimated to be much stronger than that of related neutral **D**, owing to the presence of the Li^+ ion.

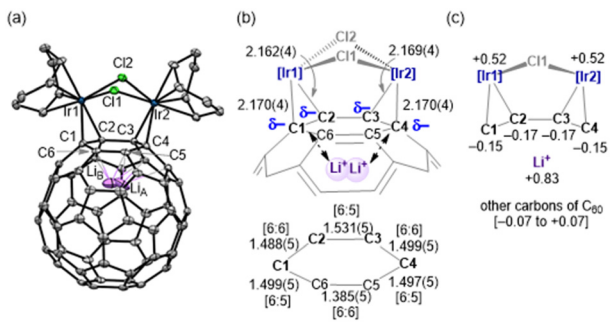

Fig. 2 (a) Molecular structure of the cationic part of **1** with thermal ellipsoids at the 50% probability level. All hydrogen atoms are omitted for clarity. The Li atom is disordered in the two sites (Li_A: Li_B = 53%: 47%). (b) Selected bond distances (Å) and schematic electronic interaction between the C_{60} shell and the encapsulated Li^+-ion. [6 : 6] and [6 : 5] denote the positions in the C_{60} shell. (c) Selected NPA charge calculated by DFT.

The endohedral Li^+-ion is disordered in two positions in dinuclear **1–3**, in contrast to mononuclear **A–C**, where the position of the Li^+-ion is fixed in a single site close to the metal (1.54–1.57 Å away from the C_{60} centroid).[9] The averaged position is shifted to the metal fragment from the C_{60} centroid by av. 1.56 (**1**), 1.55 (**2**) and 1.58 (**3**) Å, reflecting the considerable electrostatic interaction between the Li^+ ion and the C_{60} cage [Fig. 2(b) and (c)]. The disordering of the Li^+ ion in two positions can be caused by the presence of two sets of the negatively charged C–C bonds attached to the diiridium unit and/or the electrostatic effect of the counter ion (The closest distance between Li_A and atoms (F3B and O3C) of NTf_2^- for **1** is 5.6 Å). In other words, the disordering of the Li^+-ion of **1–3** was restricted to only near the two metal sites, in contrast to the endohedral Li^+-ion in the $Li^+@C_{60}$ salts, which were disordered at multiple sites.[7a,b] Relevant restricted disordering of the Li^+-ion has also been reported for $Li^+@C_{60}$–Cu_4 polymer.[13] The occurrence of such disordering is an interesting issue in the chemistry of $Li^+@C_{60}$[7,14] because the positional change of the Li^+ ion by the action of external perturbation is expected to apply to molecular electronics, such as the recently reported multiple-conductivity switching of $Li^+@C_{60}$.[15]

It should be noted that the two halogen ligands, X1 and X2, are inequivalently bridged over the two iridium atoms in complexes **1–3**: X1 and X2 are located at the *endo*- and *exo*-positions, respectively, with respect to the coordinated six-membered ring of C_{60}. The Ir–X2 distances [av. 2.5433(7) (**1**), 2.6459(4) (**2**) and 2.7676(4) (**3**) Å] are longer than those of Ir–X1 [av. 2.3990(6) (**1**), 2.5262(4) (**2**) and 2.6803(5) (**3**) Å] by *ca.* 0.1 Å. The average Ir–X1/X2 bond distances are elongated by about 0.1–0.2 Å in the order of Cl < Br < I, in accordance with the ionic radii of the halogens (Cl = 1.81, Br = 1.96 and I = 2.20 Å).[16] Oppositely, the Ir–X–Ir bond angle decreases in this order (Table S2, ESI†). These structural differences are small but may influence their electronic structures.

The high solubility of complexes **1–3** in CD_2Cl_2 allowed us to investigate their properties in solution. In the ^7Li NMR spectra of **1–3**, all the signals of the Li^+ ion were observed exactly at δ −11.0, which is shifted up-field by 0.9 ppm from that of $[Li^+@C_{60}](NTf_2^-)$ (δ −10.1), due to the coordination of the $Li^+@C_{60}$ cage to the metal fragment. This up-field shift of the signal is comparable with those reported for mononuclear complexes **A** (δ −11.6), **B** (δ −11.0) and **C** (δ −10.8).[9] The ^1H NMR spectra of **1–3** at room temperature (300 K) showed multiple broadened signals assignable to the cod ligand in the

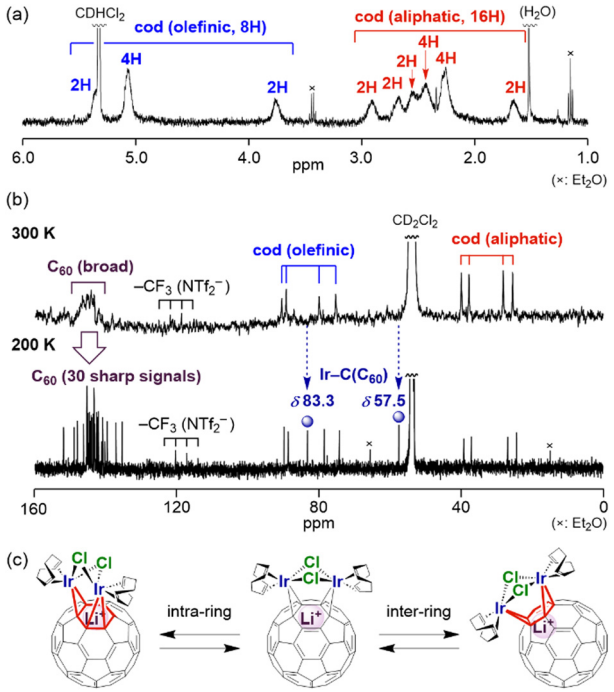

Fig. 3 (a) ^{1}H NMR spectrum of **1** in CD_2Cl_2 (400 MHz, 300 K). (b) $^{13}C\{^{1}H\}$ NMR spectra of **1** in CD_2Cl_2 at 300 and 200 K (101 MHz). (c) A possible mechanism for the dynamic behaviour of **1** *via* haptotropic rearrangements.

region of δ 1.5–5.5 [Fig. 3(a)]. The two cod ligands were observed to be equivalent, indicating that the complex had a C_s-symmetric structure with a pseudo-mirror plane passing through the two halogen atoms and the Li^+-ion in solution. In the ^{13}C NMR spectrum at 300 K [Fig. 3(b)], a very broad signal was observed in the C_{60} carbon region (δ 140–150), implying fluxional behaviour. Upon decreasing the temperature to 200 K, the broad signal was separated into 30 singlets among the expected 32 signals in theory (28 singlets at δ 135–155 and two singlets at δ 55–85), two of which must overlap (δ 145.4 and 143.4). The two signals observed at δ 83.3 and 57.5, which are considerably shifted up-field compared with those of other C_{60} and are assigned to the carbons bonded to the Ir atoms. A similar up-field shift was observed for **B** (δ 76.8) and **C** (δ 76.1).[9] The signal change of the C_{60}-carbons between 300 and 200 K was likely driven by haptotropic rearrangements, where the diiridium unit migrated over the surface of the fullerene cage by changing the positions of the coordination bonds with C_{60} carbons between intra- or inter-rings [Fig. 3(c)].[9,17]

The UV/Vis spectra of **1–3** measured in CH_2Cl_2 exhibited three extensive absorption bands (at *ca.* 330, 420 and 530 nm), together with a very weak shoulder-like band extending to *ca.* 800 nm in all cases (see Fig. S20 in ESI†). As a representative example, the two bands at 327 and 530 nm of **1** are assigned to π–π^* transitions, although some contributions from the Ir d-orbitals are present, according to TD-DFT calculations (calcd. λ_{max} = 331 nm, f = 0.109 and 541 nm, f = 0.032 for **1**, see ESI†). These two bands were comparable to those observed for Ir complex **A** (λ_{max} = 331 and 582 nm).[9] The other band at 416 nm was assigned to a metal-to-ligand charge transfer (MLCT) transition (calcd. λ_{max} = 424 nm, f = 0.082). The last very weak band is assignable to HOMO → LUMO (*vide infra*), which should be an almost forbidden transition (calcd. λ_{max} = 689 nm, f = 0.002 for **1**). Interestingly, the absorption coefficients of the bands at longer wavelengths (*ca.* 420, 530 and 700 nm) slightly increased and red-shifted in descending order of the halogen atoms, suggesting some contribution from the halogen orbitals to the transitions (*vide infra*).

The cyclic voltammograms of **1–3** were recorded in *o*-DCB (Fig. S21 and S22, ESI†). All the complexes exhibited one set of oxidation peaks with slight cathodic shifts in the oxidation potentials from **1** ($E_{1/2}$ = +1.00 V) to **2** ($E_{1/2}$ = +0.84 V) and **3** ($E_{1/2}$ = +0.86 V). In contrast, **1–3** displayed five reduction peaks accompanied by peaks originating from free $Li^+@C_{60}$ (Fig. S22, ESI†), implying the occurrence of a dissociation equilibrium between the fullerene cage and metal units in solution under reductive conditions.

To obtain further insight into the electronic structures of **1–3**, we performed orbital analysis of their cationic parts using DFT calculations [B3PW91-D3/SDD for Ir and I, 6-311+G(d,p) for others//B3PW91/Lanl2DZ for Ir and I, and 6-31G(d) for others]. As depicted in Fig. S26–S28 in the ESI,† the three complexes have analogous orbitals. Thus, the important orbitals of chlorido complex **1** are shown in Fig. 4 as representatives. Both the HOMO and HOMO–1 of **1** consist of a C_{60} π-orbital combined with the d-orbitals of two iridium atoms in a bonding fashion and the p-orbital of one of the two bridging halogen atoms (Cl2 atom). In contrast, the LUMO of **1** represents the π^*orbitals localised in the C_{60} shell. The LUMO+1 consists of the C_{60} π^*-orbital combined with the d-orbitals of two Ir atoms in an antibonding fashion, accompanied by a slight contribution from the bridging halogen orbitals. The participation of the Ir d-orbitals and halogen p-orbitals in the fullerene π system is also found in other bonding and antibonding orbitals, which can be responsible for the aforementioned spectral changes among **1–3** in the UV/Vis and CV measurements, reflecting the energy differences and orbital sizes of 3p (Cl), 4p (Br) and 5p (I) of the halogen atoms. Moreover, from these frontier orbital features, it is understood that oxidation reduces the electron density of the entire molecule. In contrast, reduction occurs initially in the fullerene cage. However, over-reduction weakened the coordination of the fullerene cage to the Ir_2 unit, as observed by CV measurements.

In addition, the NPA charge distribution supported the presence of strong Ir-to-C_{60} π-back-donation in **1–3** (Fig. S29–S31, ESI†). In the case of **1**, the four carbon atoms bonded to Ir

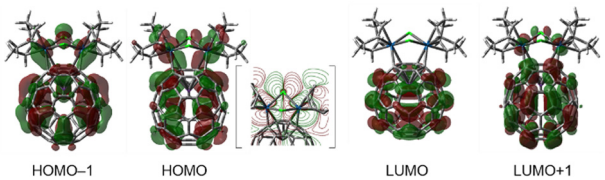

Fig. 4 Selected Kohn–Sham orbitals of **1** (isovalue = 0.02). The contour map of HOMO is inserted in the square brackets.

atoms are much more negatively charged (−0.15 to −0.17), relevant to the remaining carbons of C_{60} (−0.07 to +0.07), as illustrated in Fig. 2(c).

In summary, three diiridium complexes coordinated with Li^+-ion endohedral fullerene were successfully synthesised as soluble products in high yields (~90%). SC-XRD, DFT calculations and multiple spectroscopic techniques revealed their fundamental properties. The SC-XRD study confirmed the η^2:η^2 coordination of the $Li^+@C_{60}$ cage to the Ir_2 unit and the disordered location of the Li^+-ion at two positions adjacent to the two metal atoms. The latter observation indicated the existence of enhanced electrostatic interactions between the Li^+ cation and the negatively charged carbon atoms caused by strong π-back-donation from the two metal centres to the C_{60} cage, which was supported by DFT calculations. The ^{7}Li NMR spectra supported the coordination of the $Li^+@C_{60}$ cage to the metal fragment. ^{1}H and VT ^{13}C NMR studies revealed dynamic behaviours, including haptotropic rearrangements. Moreover, UV/Vis and CV characteristics and DFT calculations suggest significant orbital interactions among the C_{60} π-system, the d-orbitals of diiridium, and the p-orbitals of the bridging halogen atoms. The development of electron transporting materials based on complexes **1–3** is currently underway.

This research was supported by JSPS KAKENHI Grants JP22K05123 and JP22H02088 from the Japan Society for the Promotion of Science (JSPS). We thank Dr H. Sato (Rigaku Corporation, Tokyo, Japan) for his support in XRD study and acknowledge the Research and Analytical Center for Giant Molecules, Tohoku University, for high-resolution mass spectroscopy and elemental analysis. The computation was performed at the Research Center for Computational Science, Okazaki, Japan (Project: 23-IMS-C246 and 24-IMS-C260). The authors are grateful to Idea International Co, Ltd, for providing the $Li^+@C_{60}$ salt sample. One of the authors (C. F.) thanks the Tohoku University Division for Interdisciplinary Advanced Research and Education (DIARE) for scholarship support.

Data availability

The data supporting this article have been included in the ESI.†

Conflicts of interest

There are no conflicts to declare.

Notes and references

1 (*a*) O. Maury and H. L. Bozec, *Acc. Chem. Res.*, 2005, **38**, 691–704; (*b*) W. C. H. Choy, W. K. Chan and Y. Yuan, *Adv. Mater.*, 2014, **26**, 5368–5399.
2 (*a*) X. Wan, C. Li, M. Zhang and Y. Chen, *Chem. Soc. Rev.*, 2020, **49**, 2828–2842; (*b*) Y. Tanaka, *Dalton Trans.*, 2024, **53**, 8512–8523.
3 (*a*) C. K. Prier, D. A. Rankic and D. W. C. MacMillan, *Chem. Rev.*, 2013, **113**, 5322–5363; (*b*) F. Glaser and O. S. Wenger, *Coord. Chem. Rev.*, 2020, **405**, 213129.
4 (*a*) A. L. Balch and M. M. Olmstead, *Chem. Rev.*, 1998, **98**, 2123–2166; (*b*) M. A. Lebedeva, T. W. Chamberlain and A. N. Khlobystov, *Chem. Rev.*, 2015, **115**, 11301–11351; (*c*) A. L. Balch and K. Winkler, *Chem. Rev.*, 2016, **116**, 3812–3882; (*d*) D. V. Konarev and R. N. Lyubovskaya, *Russ. Chem. Rev.*, 2016, **85**, 1215–1228; (*e*) A. L. Balch and K. Winkler, *Coord. Chem. Rev.*, 2021, **438**, 213623; (*f*) D. V. Konarev, S. S. Khasanov, A. F. Shestakov, M. Ishikawa, A. Otsuka, H. Yamochi, G. Saito and R. N. Lyubovskaya, *J. Am. Chem. Soc.*, 2016, **138**, 16592–16595; (*g*) D. V. Konarev, A. V. Kuzmin, S. S. Khasanov, S. I. Troyanov, A. Otsuka, H. Yamochi, H. Kitagawa and R. N. Lyubovskaya, *Organometallics*, 2017, **36**, 4032–4037; (*h*) T. Tanase, K. Nakamae, Y. Kitagawa and T. Nakajima, *Chem. Eur. J.*, 2021, **27**, 12953–12958; (*i*) S.-Z. Zhan, G.-H. Zhang, J.-H. Li, J.-L. Liu, S.-H. Zhu, W. Lu, J. Zheng, S. W. Ng and D. Li, *J. Am. Chem. Soc.*, 2020, **142**, 5943–5947; (*j*) S.-Z. Zhan, Y.-L. Liu, H. Cai, M.-D. Li, Q. Huang, X.-D. Wang, M. Li, L. Dang, S. W. Ng, W. Lu and D. Li, *Angew. Chem., Int. Ed.*, 2023, **62**, e202312698; (*k*) Y. Hashikawa, H. Kawasaki and Y. Murata, *Organometallics*, 2022, **41**, 354–359; (*l*) Y. Hashikawa and Y. Murata, *Organometallics*, 2024, **43**, 227–232.
5 (*a*) A. Hirsch, I. Lamparth and H. R. Karfunkel, *Angew. Chem., Int. Ed. Engl.*, 1994, **33**, 437–438; (*b*) A. L. Balch, J. W. Lee, B. C. Noll and M. M. Olmstead, *Inorg. Chem.*, 1994, **33**, 5238–5243.
6 N. O. Mchedlov-Petrossyan, *Chem. Rev.*, 2013, **113**, 5149–5193.
7 (*a*) S. Aoyagi, E. Nishibori, H. Sawa, K. Sugimoto, M. Takata, R. Kitaura, H. Shinohara, H. Okada, T. Sakai, Y. Ono, K. Kawachi, K. Yokoo, S. Ono, K. Omote, Y. Kasama, S. Ishikawa, T. Komuro and H. Tobita, *Nat. Chem.*, 2010, **2**, 678–683; (*b*) S. Aoyagi, Y. Sado, E. Nishibori, H. Sawa, H. Okada, H. Tobita, Y. Kasama, R. Kitaura and H. Shinohara, *Angew. Chem., Int. Ed.*, 2012, **51**, 3377–3381.
8 H. Okada, T. Komuro, T. Sakai, Y. Matsuo, Y. Ono, K. Omote, K. Yokoo, K. Kawachi, Y. Kasama, S. Ono, R. Hatakeyama, T. Kaneko and H. Tobita, *RSC Adv.*, 2012, **2**, 10624–10631.
9 T. Watanabe, M. F. Itoh, T. Komuro, H. Okada, T. Sakai, Y. Ono, K. Kawachi, Y. Kasama and H. Tobita, *Organometallics*, 2014, **33**, 608–611.
10 (*a*) M.-C. Yang, A. K. Sharma, W. M. C. Sameera, K. Morokuma and M.-D. Su, *J. Phys. Chem. A*, 2017, **121**, 2665–2673; (*b*) M.-C. Yang and M.-D. Su, *ACS Omega*, 2019, **4**, 3105–3113.
11 H. Okada and Y. Matsuo, *Fullerenes, Nanotubes Carbon Nanostruct.*, 2014, **22**, 262–268.
12 M. Rasinkangas, T. T. Pakkanen, T. A. Pakkanen, M. Ahlgrén and J. Rouvinen, *J. Am. Chem. Soc.*, 1993, **115**, 4901.
13 Y. Shen, M. Cui, S. Takaishi, H. Kawasoko, K. Sugimoto, T. Tsumuraya, A. Otsuka, E. Kwon, T. Yoshida, N. Hoshino, K. Kawachi, Y. Kasama, T. Akutagawa, T. Fukumura and M. Yamashita, *Nat. Commun.*, 2022, **13**, 495.
14 (*a*) S. Aoyagi, A. Tokumitu, K. Sugimoto, H. Okada, N. Hoshino and T. Akutagawa, *J. Phys. Soc. Jpn.*, 2016, **85**, 094605; (*b*) S. Aoyagi, K. Miwa, H. Ueno, H. Okada, Y. Matsuo and K. Kokubo, *R. Soc. Open Sci.*, 2018, **5**, 180337; (*c*) H. Suzuki, M. Ishida, M. Yamashita, C. Otani, K. Kawachi, Y. Kasama and E. Kwon, *Phys. Chem. Chem. Phys.*, 2016, **18**, 31384–31387; (*d*) H. Suzuki, M. Ishida, C. Otani, K. Kawachi, Y. Kasama, E. Kwon, Y. Miyazaki and M. Nakano, *Phys. Chem. Chem. Phys.*, 2019, **21**, 16147–16153; (*e*) H. Ando and Y. Nakao, *Phys. Chem. Chem. Phys.*, 2021, **23**, 9785–9803; (*f*) H. Ando and Y. Nakao, *Phys. Chem. Chem. Phys.*, 2023, **25**, 8446–8462.
15 (*a*) H. J. Chandler, M. Stefanou, E. E. B. Campbell and R. Schaub, *Nat. Commun.*, 2019, **10**, 2283; (*b*) A. K. Ismael, *ACS Omega*, 2023, **8**, 19767–19771.
16 R. D. Shannon, *Acta Crystallogr. A*, 1976, **32**, 751–767.
17 (*a*) M. L. H. Green and A. H. H. Stephens, *Chem. Commun.*, 1997, 793–794; (*b*) I. D. Gridnev, *Coord. Chem. Rev.*, 2008, **252**, 1798–1818.

